JOURNAL OF BACTERIOLOGY, Dec. 2009, p. 7531–7537 Vol. 191, No. 24
0021-9193/09/$12.00 doi:10.1128/JB.00631-09
Copyright © 2009, American Society for Microbiology. All Rights Reserved.

Structural Plasticity and Distinct Drug-Binding Modes of LfrR, a Mycobacterial Efflux Pump Regulator▽

Marco Bellinzoni,[1] Silvia Buroni,[2] Francis Schaeffer,[1] Giovanna Riccardi,[2] Edda De Rossi,[2] and Pedro M. Alzari[1]*

Institut Pasteur, Unité de Biochimie Structurale and CNRS URA2185, 75724 Paris Cedex 15, France,[1] and Dipartimento di Genetica e Microbiologia, Università degli Studi di Pavia, 27100 Pavia, Italy[2]

Received 13 May 2009/Accepted 29 September 2009

The TetR-like transcriptional repressor LfrR controls the expression of the gene encoding the *Mycobacterium smegmatis* efflux pump LfrA, which actively extrudes fluoroquinolones, cationic dyes, and anthracyclines from the cell and promotes intrinsic antibiotic resistance. The crystal structure of the apoprotein form of the repressor reveals a structurally asymmetric homodimer exhibiting local unfolding and a blocked drug-binding site, emphasizing the significant conformational plasticity of the protein necessary for DNA and multidrug recognition. Crystallographic and calorimetric studies of LfrR-drug complexes further confirm the intrinsic flexibility of the homodimer, which provides a dynamic mechanism to broaden multidrug binding specificity and may be a general property of transcriptional repressors regulating microbial efflux pump expression.

The increase in multidrug resistance among both gram-positive and gram-negative pathogenic bacteria is emerging as a major problem in human health (15). Classical resistance mechanisms include enzymatic inactivation of the antibiotic as well as modification of either the drug target(s) or enzymes involved in prodrug activation. Another important mechanism that contributes to the spread of multidrug resistance is the overexpression of multidrug efflux pumps, which are able to extrude many different molecules (including clinically relevant antimicrobials) from the bacterial cell (2). Efflux mechanisms are key determinants of both intrinsic and acquired antibiotic resistance in major human pathogens, such as *Pseudomonas aeruginosa* and *Staphylococcus aureus* (27, 28), raising important questions about the molecular basis of multidrug recognition by both the transmembrane efflux pumps and their associated cytoplasmic regulatory proteins.

The intrinsic resistance of *Mycobacterium tuberculosis*, the etiological agent of tuberculosis, to most antibiotics is generally attributed both to the low permeability of the mycobacterial cell wall (3, 25) and to active efflux systems that extrude the drug molecules from the cells (10). However, although several efflux pumps have been identified and characterized in mycobacteria (11, 22, 29, 30, 41), their involvement in intrinsic and acquired drug resistance remains unclear (10). The first efflux pump described in mycobacteria, *Mycobacterium smegmatis* LfrA, belongs to the major facilitator superfamily and was identified in an *M. smegmatis* strain where its overexpression conferred resistance to ciprofloxacin (38). It was subsequently shown that overexpression of the *lfrA* gene conferred resistance not only to various hydrophilic fluoroquinolones but also to acriflavine and ethidium bromide (23, 38), and these observations were further confirmed by *lfrA* gene inactivation in *M. smegmatis* (32).

The *lfrA* gene is transcriptionally regulated by the TetR-like repressor LfrR (6). Deletion of the *lfrR* gene significantly increased *lfrA* expression and rendered *M. smegmatis* markedly more resistant to ciprofloxacin, norfloxacin, ethidium bromide, and acriflavine, all typical substrates of the LfrA efflux pump (22). Furthermore, different LfrA substrates were shown to upregulate the expression of the transporter by specifically promoting the dissociation of the repressor-operator complex. Thus, as documented for the *Staphylococcus aureus* efflux pump regulator QacR (33), these data strongly suggest that LfrR matches the broad multidrug binding specificity of LfrA. To gain further insight into the molecular basis of these functional properties, we report here structural and binding studies of mycobacterial LfrR.

MATERIALS AND METHODS

Plasmid construction. The construction of the pET-15b/*lfrR* expression plasmid has been described previously (6). To obtain a construct allowing the cleavage of the N-terminal His_6 tag with tobacco etch virus (TEV) protease, the *lfrR* gene was amplified from the pET-15b/*lfrR* construct with the following primers, each including an EcoRI recognition site: 5′-ATTAAGAATTCGAGAATCTTTATTTTCAAGGAATGACCAGCCCGAGCATCG-3′ (forward), which carries a 21-nucleotide sequence (underlined) encoding the optimal TEV cutting site Glu-Asn-Leu-Tyr-Phe-Gln-Gly, and 5′-TTTAAGAATTCAGGTGCGCGGCAGGGTG-3′ (reverse). The purified PCR product was cut with EcoRI, purified on a Qiaquick column (Qiagen), and ligated into the pET-28a vector, leading to the pET-28a/*lfrR* construct.

Protein expression and purification. The pET-15b/*lfrR* or pET-28a/*lfrR* construct was introduced into the *E. coli* strain BL21(DE3)pLysS (Novagen). Recombinant LfrR-His_6 was overexpressed from pET-15b/*lfrR* as described previously (6). Cultures of the pET28a/*lfrR*-transformed strain were instead grown at 30°C to an optical density at 600 nm of 0.8, and expression of the recombinant protein was induced by the addition of 0.5 mM isopropyl-β-thio-galactopyranoside (IPTG); growth was then continued for a further 4 h at 30°C. Bacteria were harvested by centrifugation at 5,000 × *g* for 20 min, washed with phosphate-buffered saline (140 mM NaCl, 2.7 mM KCl, 10 mM Na_2HPO_4, 1.8 mM KH_2PO_4 [pH 7.3]), and stored at −80°C.

The same purification protocol was carried out for both constructs, except for the TEV cleavage step, which could not be performed for the protein expressed from the pET-15b/*lfrR* construct. Frozen cells were thawed, resuspended in lysis

* Corresponding author. Mailing address: Institut Pasteur, Unité de Biochimie Structurale and CNRS URA 2185, 25 rue du Dr. Roux, 75724 Paris Cedex 15, France. Phone: 33-1-45688607. Fax: 33-1-45688604. E-mail: pedro.alzari@pasteur.fr.

▽ Published ahead of print on 9 October 2009.

buffer (50 mM NaH_2PO_4, 500 mM NaCl, 25 mM imidazole, 5% glycerol [pH 8.0]), and lysed by sonication on ice. The lysate obtained from 6.4 liters of bacterial culture was centrifuged at 26,800 × *g* for 1 h, filtered (pore size, 0.45 μm), and loaded onto a 5-ml HisTrap Ni^{2+}-IMAC column (GE Healthcare). Recombinant LfrR was eluted by applying a 25 to 400 mM imidazole gradient in the same buffer; the fractions containing the recombinant protein, as confirmed by sodium dodecyl sulfate-polyacrylamide gel electrophoresis (SDS-PAGE), were pooled and dialyzed overnight at 4°C against 50 mM Tris-HCl (pH 8.0)–150 mM NaCl–10% glycerol. To cleave the affinity tag, recombinant TEV protease, prepared as described previously (40), was added to a final mass ratio of 1:30 to the pool of fractions before dialysis, which was carried out at 22°C for 12 h in the presence of 1 mM dithiothreitol. The digestion mixture was then passed through 1 ml of nickel-nitrilotriacetic acid resin (Qiagen) by gravity flow to separate LfrR from the cut histidine tag and the protease. Either the nickel-nitrilotriacetic acid column flowthrough (containing cleaved LfrR) or the dialyzed LfrR-His_6 was concentrated and injected onto a HiLoad 16/60 Superdex 75 gel filtration column (GE Healthcare), equilibrated in 50 mM Tris-HCl (pH 8.0)–150 mM NaCl–5% glycerol, and run at 1 ml/min. The fractions corresponding to the LfrR peak, as confirmed by SDS-PAGE, were pooled and concentrated up to 44 mg/ml (LfrR-His_6) or 128 mg/ml (LfrR) with 3-kDa-cutoff Vivaspin concentrators (Sartorius). The concentrated protein, with a purity of >95% as estimated by Coomassie blue staining after SDS-PAGE, was flash-frozen in liquid nitrogen and stored at −80°C.

Crystallization. Crystals of LfrR-His_6 in free form were obtained by the hanging drop vapor diffusion method by mixing 2 μl of purified protein at 44 mg/ml with 2 μl of 10% (wt/vol) polyethylene glycol (PEG) 8000–2.0 M NaCl. Rod-like crystals appeared after 45 days at 18°C and were transferred to a cryoprotectant solution composed of 10% (wt/vol) PEG 8000, 2.0 M NaCl, and 25% (vol/vol) glycerol prior to being frozen in liquid nitrogen. To obtain a heavy-atom derivative for phasing, single crystals were soaked for 5 min at 18°C in 7.5% (wt/vol) PEG 8000–1.5 M NaCl–18.75% (vol/vol) glycerol–50 mM K_2PtCl_4 and were directly frozen in liquid nitrogen. A second crystallization condition was later identified from microdrops made with His_6-cleaved protein, in which isomorphous crystals appeared after more than 3 months in 10% PEG 8000–0.5 M $LiSO_4$; a cryoprotectant was made in this case with 7.5% PEG 8000, 0.375 M $LiSO_4$, and 25% (vol/vol) glycerol. A few crystals were harvested from drops, dissolved in water, and analyzed by SDS-PAGE and surface-enhanced laser desorption ionization–time-of-flight (SELDI-TOF) mass spectrometry to verify the absence of proteolytic degradation.

Crystals of the LfrR-proflavine complex were obtained by the sitting-drop method from 64 mg/ml LfrR (without a His_6 tag) preincubated overnight with 2.5 mM acriflavine (Sigma) and were mixed with an equal volume of 2.0 M $(NH_4)_2SO_4$–5% (vol/vol) isopropanol. Crystals appeared after 2 months at 18°C and were washed into 1.5 M $(NH_4)_2SO_4$–3.75% (vol/vol) isopropanol–25% (vol/vol) glycerol as the cryoprotectant before being frozen in liquid nitrogen.

Data collection, structure solution, and refinement. All diffraction data sets were collected at the ESRF synchrotron (Grenoble, France) from single crystals at 100 K, processed with XDS (19), and scaled either with XSCALE from the XDS package or with SCALA from the CCP4 suite (7). To solve the structure of the repressor in the free form, a platinum derivative was successfully generated after a 5-min soak in a cryoprotectant solution containing 50 mM K_2PtCl_4 (see above). A two-wavelength anomalous diffraction (multiwavelength anomalous diffraction [MAD]) data set was then collected at the ID23-1 beamline at the energies corresponding, respectively, to the Pt L_{III} edge peak (E = 11,556.0 eV; λ = 1.0729 Å) and inflection point (E = 11,551.7 eV; λ = 1.0733 Å), as determined by a fluorescence scan. Two Pt sites per asymmetric unit were located with SHELXD (37) from the anomalous signal in the peak data set; subsequent heavy-atom site refinement, two-wavelength MAD phasing, and density modification were carried out with autoSHARP (42). The electron density map calculated with the solvent-flipped phases at 2.8 Å resolution allowed the manual tracing of the model with the Coot program (14), alternated with restrained refinement with REFMAC5 (24). The model was then further refined on a 2.0-Å-resolution data set collected from an isomorphous crystal at the ESRF beamline ID23-2. The structure of the triclinic LfrR-proflavine complex, whose diffraction data at 1.9 Å resolution were collected at the ESRF beamline ID14-2, was solved by molecular replacement with the MOLREP program (39) by using the structure of the LfrR dimer without the N-terminal helix-turn-helix domains as the search model. To remove the residual bias from the starting model, density modification with solvent flipping was carried out with the CNS suite (5), starting from phases calculated from the molecular replacement solution and applying noncrystallographic symmetry averaging between the two LfrR dimers in the asymmetric unit. The resulting electron density map allowed manual rebuilding with COOT, alternated with refinement with REFMAC5; once the main chain was fully traced, unambiguous electron density for a proflavine molecule per dimer appeared in sigma A-weighted Fourier difference maps. The refinement of both LfrR models was completed with phenix.refine (1) with a TLS (translation/libration/screw) model. The geometry of all models was validated with the Molprobity server (http://molprobity.biochem.duke.edu) (8). Data collection and refinement statistics are reported in Table 1. Figures were generated and rendered with Pymol (http://www.pymol.org) (9); electrostatic surfaces were rendered with the APBS plugin within Pymol, supplying atomic charges and radii calculated through the "PDB2PQR" server (http://pdb2pqr.sourceforge.net) (13) by applying the CHARMM force field.

ITC. LfrR-ligand interactions were quantified thermodynamically using the VP-ITC system (MicroCal Inc., MA). The isothermal titration calorimetry (ITC) cell contained 32 μM LfrR (His_6 tag free) in 50 mM Tris-HCl (pH 8.0)–150 mM NaCl–5% glycerol, while the syringe contained either 553 μM proflavine, 350 μM rhodamine 123, or 265 μM ethidium bromide, dissolved in the same buffer. Protein and ligand concentrations in the final solutions were verified spectrophotometrically by measuring the absorbance at a λ of 280 nm for LfrR, 444 nm for proflavine, 511 nm for rhodamine 123, and 480 nm for ethidium bromide. Sample solutions were thoroughly degassed under vacuum, and each titration was performed at 25°C by 1 injection of 2 μl followed by 29 injections of 10 μl, with a 210-s interval between injections and constant stirring (290 rpm). The raw heat signal collected with a 16-s filter was corrected for the dilution heat of the ligand and normalized to the concentration of ligand injected. Data were fit either to a single binding site or to a two-site model (16) by using the ORIGIN software provided by the manufacturer. Thermodynamic parameter values for binding are reported, with error bars corresponding to variations from the means of two independent titrations for ethidium bromide binding and to nonlinear least-square fitting errors for proflavine and rhodamine 123 binding, calculated using the Levenberg-Marquardt iteration method as implemented in ORIGIN.

Protein structure accession numbers. Atomic coordinates and structure factors have been deposited in the Protein Data Bank (PDB) with accession codes 2WGB (LfrR apoprotein form) and 2V57 (LfrR-proflavine).

RESULTS

Structure of unbound LfrR. The 3-dimensional structure of recombinant LfrR was determined using a MAD approach on a platinum derivative and was refined at 2.0 Å resolution to a final *R* of 0.185 (R_{free} = 0.228) (Table 1). The structure revealed a homodimer displaying the canonical Ω shape, an entirely α-helical architecture characteristic of the TetR-like transcriptional repressors. Each monomer is made up of nine α-helices (Fig. 1A), of which the first three (residues Ala10 to Pro53) define the N-terminal DNA-binding domain (DBD), which includes a helix-turn-helix motif (helices α2 and α3). The C-terminal helices define the ligand-binding and dimerization domain (LBD) (31). The architecture of the LBD can be described as composed of three helical "layers" (Fig. 1A): the first (inner) layer is composed of helices α8 and α9, which are mostly involved in protein dimerization; the intermediate layer is composed of helices α5, α6, α7a, and α7b; and the outer layer includes helix α4, to which the DBD is attached.

In contrast with the high internal symmetry characteristic of ligand-free TetR-like homodimers, the overall structure of LfrR is strikingly asymmetric (Fig. 1B). All equivalent Cα atoms from both monomers can be superimposed with a root mean square deviation (RMSD) of 3.4 Å. The largest differences are seen for the region between Leu98 and Pro140 (within the intermediate helical layer), which in monomer A folds into two short helices (α6, α7b) connected by a long loop protruding toward the opposite monomer (Fig. 1A and B). The structural changes in this region promote a significant reorientation of helices α1 to α4, which move as a rigid body pivoting on the C terminus of helix α4 (Fig. 1B). Due to steric clashes at the monomer-monomer interface, the particular conformation of the loop 105-114 in monomer A is incompatible with

TABLE 1. Diffraction data collection and refinement statistics

Statistic	LfrR apoprotein			LfrR-proflavine
	Pt derivative		Native	
	Peak	Inflection point		
Data collection				
Beamline	ESRF ID23-1	ESRF ID23-1	ESRF ID23-2	ESRF ID14-2
Space group	$P4_12_12$		$P4_12_12$	P1
X-ray wavelength (Å)	1.0729	1.0733	0.8726	0.9330
Cell dimensions a, b, c (Å)	86.2, 86.2, 96.9		86.6, 86.6, 96.8	48.3, 62.4, 70.6
α, β, γ (°)	90.00, 90.00, 90.00		90.00, 90.00, 90.00	63.88, 88.34, 88.13
Resolution (Å)[a]	20.0–2.6 (2.80–2.60)	20.0–2.8 (3.00–2.80)	48.4–2.0 (2.11–2.00)	48.3–1.9 (2.00–1.90)
No. of unique reflections[b]	21,326	17,190	25,569	56,578
$I/\sigma(I)$[a]	12.4 (3.8)	10.1 (2.2)	31.6 (5.9)[c]	11.4 (2.4)[c]
Multiplicity[a]	3.8 (3.8)	3.8 (3.8)	14.5 (14.7)	2.1 (2.1)
Completeness (%)[a]	99.4 (97.4)	99.9 (100.0)	100.0 (100.0)	96.9 (95.7)
R_{merge}[a,d]	0.097 (0.375)	0.149 (0.659)	0.063 (0.515)[c]	0.050 (0.384)[c]
Phasing power[e]	1.00	0.42		
Refinement				
No. of reflections used[f]			24,235	53,733
R factor/R_{free}[g]			0.185/0.228	0.196/0.234
RMSD bond length (Å)			0.007	0.008
RMSD bond angle (°)			0.825	1.009
% Ramachandran favored regions			98.7	99.4
% Ramachandran allowed regions			0.9	0.6
Average atomic B factor (Å^2)				
Protein			39.8	29.9
Ligand (proflavine)				26.1
Solvent			41.6	37.6

[a] Numbers in parentheses correspond to the outer resolution shell.
[b] Friedel mates are unmerged for Pt derivative data sets.
[c] Cutoff criteria for reflections are as follows: $\langle I/\sigma(I)\rangle > 2.0$ and $R_{merge} \leq 0.50$ (see below).
[d] $R_{merge} = \{\Sigma_j|\hat{I}_h - I_{h,j}|\}/\Sigma_{h,j} I_{h,j}$, where $\hat{I}_h = (\Sigma_j I_{h,j})/n_h$ and n_h is the multiplicity of reflection h.
[e] Phasing power = $\langle F_h$ (calc) /phase-integrated lack of closure$\rangle$.
[f] The R_{free} set of reflections is not included (5% of total reflections).
[g] R factor = $\Sigma_{hkl} \|F_o| - k|F_c\|/\Sigma_{hkl} F_o$; R_{free} is calculated in the same manner for the test set (5% of total reflections).

the formation of a symmetric homodimer. Indeed, no electron density was observed for residues 110 to 124 in monomer B, which comprise helix α7b and its flanking segments, indicating that this region is disordered in the crystal structure. SDS-PAGE and mass spectrometry analyses of crystalline material revealed that the disorder was most likely due to local unfolding, since no proteolytic degradation of the protein was detected (data not shown). In agreement with these observations, monomer B displays a significantly higher mobility, with an average B factor of 51.6 Å^2 compared to 29.9 Å^2 for the first monomer (Fig. 1C).

Database searches for structural homology emphasize the structural asymmetry of LfrR. By use of secondary-structure matching (SSM) (21), monomer B was closer than monomer A to other members of the TetR family. Among functionally characterized TetR-like repressors, the closest homologues were *Vibrio cholerae* HapR (PDB entry 2PBX) (12), and *S. aureus* QacR in complex with its DNA operator (PDB entry 1JT0) (35), with RMSD values of 2.65 Å and 2.42 Å, respectively. In contrast, all hits for monomer A displayed RMSD values above 3.0 Å, and its closest homologues were mainly structures of uncharacterized proteins from structural genomics initiatives, such as the unpublished PDB entries 2IBD (3.14 Å), 3BRU (3.20 Å), and 3F1B (3.65 Å). Using two different approaches, secondary-structure matching and Dali (18), the well-characterized QacR repressor in its DNA-bound form (1JT0) (35) was consistently reported among the best hits for each LfrR monomer. Since the asymmetrical region of LfrR matches a region in QacR that undergoes significant rearrangement upon ligand binding (36), we therefore sought to determine the structural effects of ligand binding to LfrR.

Structure of the proflavine complex. Extensive cocrystallization screenings of LfrR in complex with either acriflavine/proflavine, ethidium bromide, or rhodamine 123 failed to produce crystals. A new LfrR construct, including a protease cleavage site to excise the N-terminal His_6 tag, was therefore generated, and triclinic crystals of the tag-free repressor in complex with proflavine were eventually obtained. The structure of the complex was determined by molecular replacement and was refined at 1.9 Å resolution to a final R of 0.196 and an R_{free} of 0.234 (Table 1). The final model contains two LfrR homodimers in the asymmetric unit, which are very similar to each other and could indeed be refined by applying noncrystallographic symmetry restraints. Instead, each homodimer still displays significant internal conformational asymmetry; the two monomers can be superimposed with an RMSD of 1.5 Å for equivalent Cα atoms.

This asymmetry is due mostly to drug-binding stoichiometry,

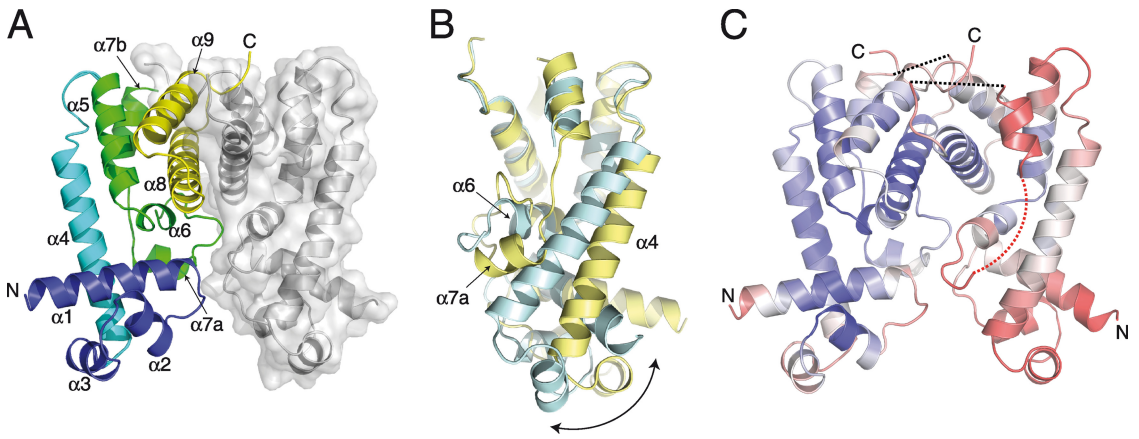

FIG. 1. (A) Cartoon diagram of the LfrR dimer in the apoprotein form. In chain A, the DBD, formed by helices α1 (residues 10 to 28), α2 (residues 34 to 41), and α3 (residues 45 to 51), is shown in blue, the external helix α4 (residues 55 to 77) in cyan, the intermediate helices α5 to α7b (residue numbers vary for each monomer; see Fig. 3 for details) in green, and the inner helices α8 (residues 146 to 163) and α9 (residues 168 to 181) in yellow. (B) Ribbon representation of the superposition of monomer A (yellow) and monomer B (cyan), viewed laterally with respect to panel A to underline the pivoting motion of helix α4 and its associated DBD (arrow). (C) Cartoon diagram colored according to B factors, with a gradient varying from blue (lowest) to red (highest). The disordered loop connecting helices α7b and α8 in both monomers is shown as a black dotted line, while disordered residues 112 to 125 in monomer B (right) are indicated by a red dotted line.

since each homodimer binds one molecule of proflavine into a wide pocket entirely defined by a single monomer chain (Fig. 2A). The bound ligand could be refined at full occupancy (Fig. 2B), but no evidence of a second bound molecule was found in the opposite monomer. The aromatic proflavine molecule lies parallel to the side chain of Trp152 in a π-π stacking interaction, and it is further stabilized by three intermolecular hydrogen bonds: two of them occur between one of the two amino groups and both oxygens of the hydroxyl group of Ser70 and the carboxyamide group of Asn71, while the third one is made by the central-ring aromatic nitrogen of proflavine and the hydroxyl group of Tyr106 (Fig. 2B). Electron density maps also indicated the presence of an additional molecule (modeled as isopropanol from the crystallization milieu) interacting with the opposite free amino group of proflavine.

The structural comparison of the apoprotein and holoprotein forms of LfrR reveals significant conformational changes. While the structures of the inner helical layer in each monomer (helices α8 and α9, involved in protein dimerization) are largely invariant (RMSDs, 0.5 to 0.7 Å), the intermediate layer (in particular helices α6, α7a, and α7b) displays the largest structural variability among the four monomers (Fig. 3A). This region is crucial for defining the drug-binding site and can indeed block the protein in a closed conformation when no ligand is present, as seen for monomer A in the apoprotein form (Fig. 3B). Furthermore, the conformation of these helices and their connecting loops are modulated by the bound ligand, as illustrated by the comparison between the two monomers in the holoprotein form of LfrR (Fig. 3C). In particular, helix α6 is longer in the ligand-free monomer (formed by residues 101 to 111) than in the ligand-bound monomer (residues 101 to 107). This drug-induced helix-to-coil transition is reminiscent

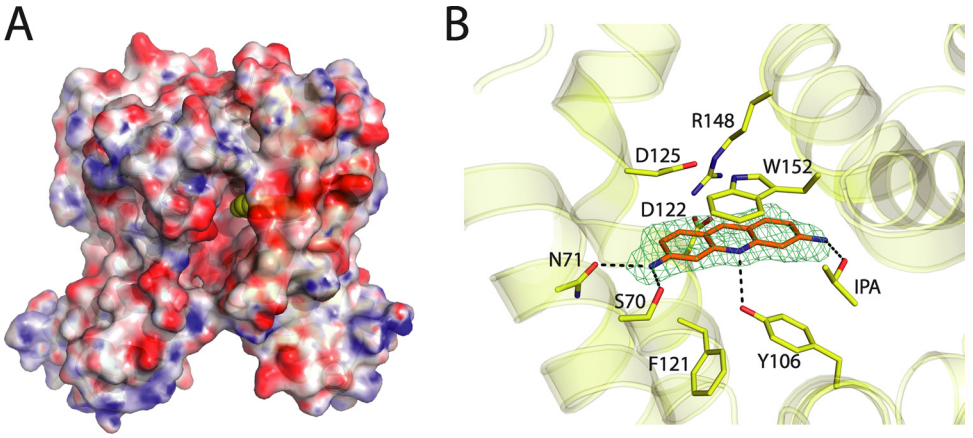

FIG. 2. (A) Front view of the LfrR dimer in complex with proflavine. The surface is colored according to the electrostatic potential. Bound proflavine is shown in yellow. (B) Drug binding pocket showing the interactions of the proflavine molecule with the surrounding residues. The sigma A-weighted difference electron density map (mF_o–DF_c), calculated before proflavine was added to the model and contoured at the 3σ level, is shown in green.

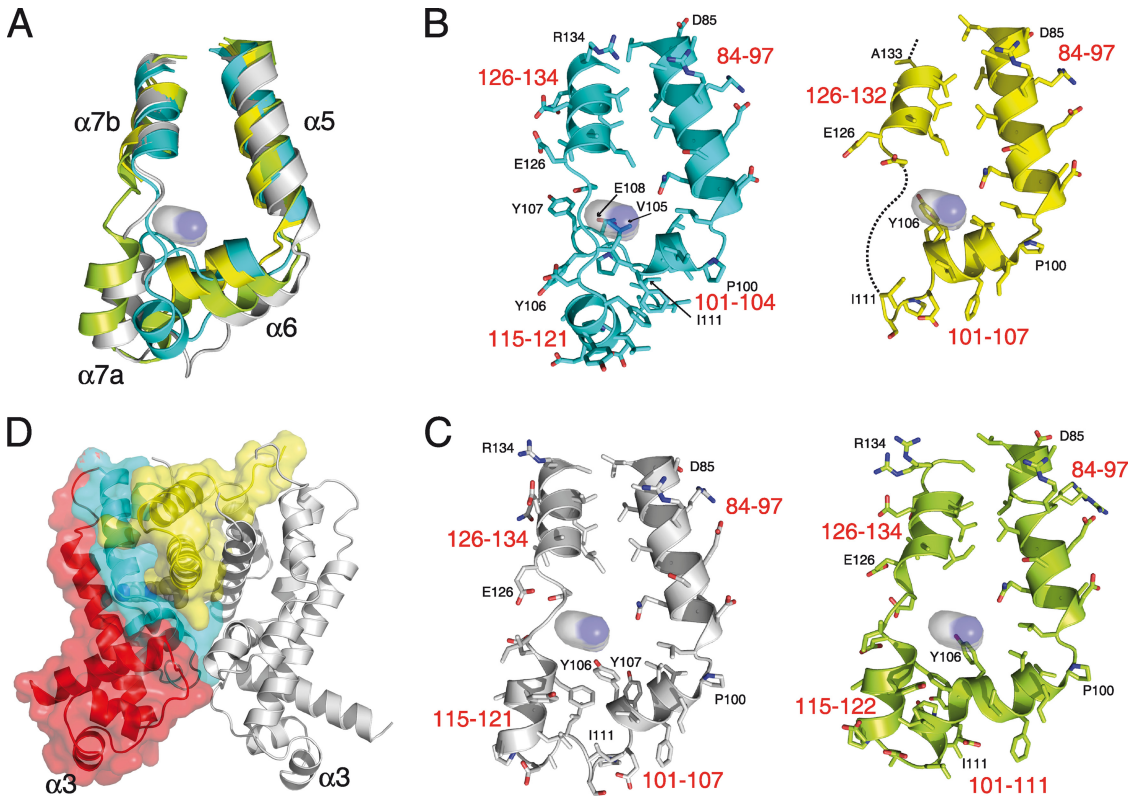

FIG. 3. (A) Superposition of helices α5, α6, α7a, and α7b, forming the intermediate helical layer in LfrR monomers, from the apoprotein form (yellow and blue) and from the holoprotein form (gray and green). (B and C) Detailed views, including side chains in each monomer, are shown for the apoprotein form (B) and the holoprotein form (C). In each case, selected residues are labeled; the ligand-binding pocket is represented by the proflavine molecule (sphere model), as seen in monomer A of the holoprotein structure; and residue positions delimiting each α-helix are indicated in red. In ligand-free monomers, the side chains of residues E108 and V105 (in monomer A of the apoprotein form) or Tyr106 (in monomer B of both the apoprotein and the holoprotein form) partially fill the volume occupied by the ligand. (D) Ribbon representation of the holoprotein form of the LfrR dimer, emphasizing the three-layer structure: inner (α8, α9) (yellow), intermediate (α5, α6, α7a, α7b) (blue), and outer (α4 plus the DBD) (red). The α3 recognition helices, which bind two consecutive major grooves of the DNA operator, are labeled. Note that the conformational changes observed in the intermediate helical layer directly modulate the relative orientation of the DBDs with respect to the central core of the dimer.

of a similar modification that was observed for *S. aureus* QacR (36), although in QacR helix α5 is elongated by one turn upon drug binding, whereas in LfrR the C terminus of helix α6 is reduced in one turn. At the end of this helix, the side chains of two adjacent tyrosine residues (Tyr106 and Tyr107) point toward the core of the dimer in both monomers. In the ligand-bound monomer, Tyr106 is engaged in a hydrogen-bonding interaction with proflavine (Fig. 2B), while Tyr107 is hydrogen bonded to the side chain of Gln156 from the opposite chain. In the absence of ligand, the side chain of Tyr106 partially occupies the drug-binding site (Fig. 3C), in analogy with the structure of QacR, where two adjacent tyrosine residues (Tyr92 and Tyr93) fulfill a similar function and were described as "drug surrogates" (36). This drug-dependent structural variability of helices α6 and α7 can directly modulate the DNA-binding capability of the repressor, because this intermediate layer of helices interacts extensively with (and determines the orientation of) helix α4 and the C-terminal end of helix α1 from the DBD (Fig. 3D).

Calorimetric studies. Drug binding studies reinforce the hypothesis of a significant plasticity and drug-dependent conformation of LfrR. The thermodynamic parameters of the repressor-drug interactions were analyzed for proflavine as well as for ethidium bromide and rhodamine 123, two additional compounds reported to induce the transcription of the *lfrA* gene (6). As shown in Fig. 4 and Table 2, all three ligands bind to LfrR with favorable binding enthalpies and binding entropies. However, significant changes in the binding stoichiometries and binding affinities are observed. LfrR titration with proflavine revealed two binding reactions depending on the ligand/protein concentration ratio. At a low molar ratio, the homodimer binds one molecule of the ligand, as seen in the crystal structure, with a high affinity constant (dissociation constant for the first reaction [$K_{d,1}$] = 79 nM). The second reaction involves the binding of two proflavine molecules per monomer, with a significantly lower binding affinity ($K_{d,2}$ = 4.3 μM). This permissive character of the drug-binding site, capable of accommodating two drug molecules simultaneously, has previously been described for *S. aureus* QacR (34). Still different behaviors were observed for LfrR titrations with ethidium bromide or rhodamine 123 (Fig. 4 and Table 2), further confirming the structural plasticity of the protein. Titration of LfrR with ethidium bromide also shows a complex isotherm. Fitting of the ethidium bromide titration curve with a two-site

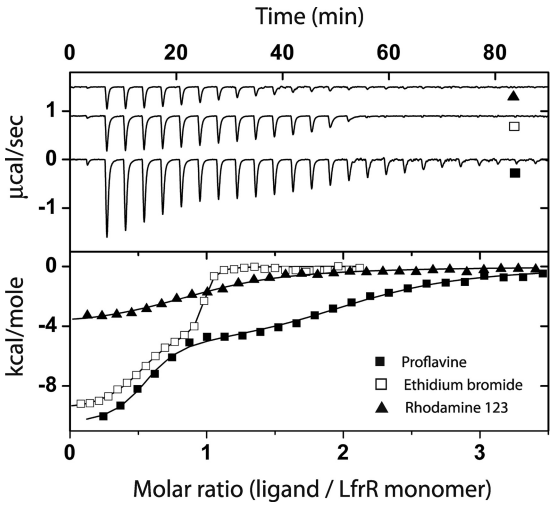

FIG. 4. ITC characterization of LfrR-ligand binding reactions. (Top) Raw heat signals for successive injections of solutions of proflavine (■), ethidium bromide (□), and rhodamine 123 (▲) into a solution of LfrR at 25°C and pH 8. (Bottom) Transition curves of the three drugs.

model shows that the binding reaction at a low molar ratio has thermodynamic parameters similar to those observed for proflavine (one ligand binding per homodimer with a high affinity [$K_{d,1}$ = 70 nM]), whereas at a higher molar ratio the ligand binds to one site per monomer with a significantly higher affinity ($K_{d,2}$ = 6 nM). Finally, the interaction of LfrR with rhodamine 123 showed a single binding reaction (Fig. 4) with one ligand binding per monomer and a weaker binding affinity (K_d = 5.0 μM).

DISCUSSION

The X-ray structure of LfrR reveals a striking asymmetry of the homodimer in the apoprotein form of the repressor, which is unusual for members of the TetR family. The analysis of more than 100 structures of TetR-like homodimers currently available in the Protein Data Bank reveals highly symmetric homodimers, either with the twofold symmetry axis of the homodimer coinciding with a crystallographic axis or with low RSMD values (<1 Å) for the superposition of the two monomers (data not shown). The only exception is the structure of the efflux pump regulator QacR from *S. aureus* in complex with drugs (4, 26, 34, 36), for which the asymmetry is due to imbalanced drug binding. The observed asymmetry in apo-LfrR, stabilized by dissimilar crystal packing contacts in the two monomers, highlights a significant conformational plasticity of the repressor. Differential packing forces can not only promote a well-defined conformation of the region spanning Leu98 to Pro140 in monomer A (which blocks the drug-binding site), but also induce the local unfolding of most of the equivalent region in the second monomer. The conformational plasticity of the repressor is further confirmed by the calorimetric studies of drug binding, since LfrR displays different modes of binding with distinct stoichiometries for the three compounds tested (Fig. 4), suggesting a high degree of protein adaptability to drug chemical structures and concentrations. Taken together, the structural and thermodynamic data strongly suggest a marginal conformational stability of the repressor in solution, particularly for the intermediate helical layer (helices α5 to α7), which serves as the structural link between the drug-binding site and helix α4 with its associated DBD (Fig. 3).

The structural adaptability of LfrR is fully consistent with the functional properties of a repressor that must deal with a large diversity of chemical compounds. Moreover, the X-ray structures of LfrR further suggest that protein adaptability also plays a key role in DNA binding. Indeed, in both the apoprotein and proflavin-bound structures, the α3 recognition helices from each monomer are separated by ~36 Å, a distance still compatible with the occupancy of two consecutive major grooves on the target DNA; as a comparison, the distance between the recognition helices in all drug-bound structures of QacR is 48 Å (36). However, the relative orientation of the DBDs in the two LfrR structures (driven by the conformation of the intermediate layer and the pivoting movement of helix α4 [Fig. 1B]) suggests that both the apoprotein and the proflavine-bound form are unlikely to represent the actual DNA-binding-competent state. Hence, the high flexibility of the apoprotein form would still allow the formation of the repressor-operator complex, whereas drug-binding could abolish DNA recognition by rigidifying LfrR, thus narrowing the conformational ensemble of the native protein that is explored during the formation of the repressor-operator complex (17, 20). Alternatively, since the ITC experiments with proflavine and ethidium bromide have shown that two binding events with distinct affinities take place per dimer, we cannot rule out the possibility that, once LfrR is bound to the *lfrRA* operator, in contrast to QacR, both binding events might be required in order to release the repressor from the DNA.

Most available structural and mechanistic insights into efflux pump regulators come from the detailed studies of *S. aureus* QacR in complex with a large diversity of compounds (4, 26, 34, 36). It is noteworthy that QacR not only is one of the closest structural homologues of LfrR but also is the only other TetR-like regulator known to bind one molecule of ligand per dimer. Similarly to the holoprotein form of LfrR, a structural reorganization of the drug-binding site in QacR takes place

TABLE 2. Thermodynamic parameters of ligand binding to the LfrR repressor at 25°C[a]

Ligand	N_1[b]	$K_{d,1}$ (nM)	ΔH_1 (kcal/mol)	$T\Delta S_1$ (kcal/mol)	N_2[b]	$K_{d,2}$ (nM)	ΔH_2 (kcal/mol)	$T\Delta S_2$ (kcal/mol)
Proflavine	0.5 ± 0.1	79 ± 25	−10.6 ± 0.3	0.9 ± 0.4	1.5 ± 0.1	4,300 ± 680	−5.4 ± 0.3	2.0 ± 0.4
Ethidium bromide	0.5 ± 0.1	68 ± 23	−4.0 ± 0.6	5.8 ± 0.8	0.5 ± 0.1	6 ± 2.5	−9.8 ± 0.8	1.5 ± 0.6
Rhodamine 123	1.0 ± 0.1	5,000 ± 790	−4.1 ± 0.2	3.2 ± 0.2				

[a] N_1 and N_2, binding stoichiometries; ΔH_1 and ΔH_2, binding enthalpies; $T\Delta S_1$ and $T\Delta S_2$, binding entropies for the first and second binding event, respectively.
[b] Binding stoichiometries refer to the LfrR monomer.

upon ligand binding. Nevertheless, in apparent contrast with the significant structural modifications observed in the apoprotein and holoprotein forms of LfrR, all available QacR-drug complexes reveal a limited reorganization of the drug-binding site, mostly associated with the exclusion of a pair of adjacent tyrosine residues (Tyr92, Tyr93) from the site and a one-turn elongation of helix α5 (33, 36). It should be emphasized, however, that all available QacR-drug complexes have been obtained in the same crystal form, suggesting that the low structural variability of QacR may to some extent be the consequence of this particular crystalline environment. This might explain both the difficulties of crystallizing QacR in its apoprotein form (i.e., due to protein flexibility) and the observation that, irrespective of their chemical nature, all drugs seem to promote the same overall structural modifications in QacR (4, 26, 34, 36).

In conclusion, the structural and thermodynamic studies of LfrR reported here suggest that the structural plasticity of the repressor, due to a marginal conformational stability in the absence of a ligand, is a crucial factor in achieving the multidrug-binding specificity associated with drug efflux function and might be a general hallmark of other efflux pump regulators. In contrast with more-specific repressors of the family, such as TetR itself, the intrinsic flexibility and the asymmetric ligand binding allow increase of the adaptive power of a single monomer to recognize a broader range of effector molecules.

ACKNOWLEDGMENTS

This work was partially supported by the European Union FP6 Project NM4TB (contract LSHP-CT-2005-018923), Institut Pasteur, CNRS (France), and FAR2007 and FAR2008 (University of Pavia).

The expression plasmid for recombinant TEV protease was kindly provided by Helena Berglund (Karolinska Institute, Stockholm, Sweden). We thank A. Haouz and P. Weber (PF6, IP) for performing robot-driven crystallization trials.

REFERENCES

1. **Afonine, P. V., R. W. Grosse-Kunstleve, and P. D. Adams.** 2005. The Phenix refinement framework. CCP4 Newsl. *42:* contribution 8. http://www.phenix-online.org/papers/ccp4_july_2005_afonine.pdf.
2. **Alekshun, M. N., and S. B. Levy.** 2007. Molecular mechanisms of antibacterial multidrug resistance. Cell **128:**1037–1050.
3. **Brennan, P. J.** 2003. Structure, function, and biogenesis of the cell wall of *Mycobacterium tuberculosis*. Tuberculosis **83:**91–97.
4. **Brooks, P. E., K. M. Piro, and R. G. Brennan.** 2007. Multidrug-binding transcription factor QacR binds the bivalent aromatic diamidines DB75 and DB359 in multiple positions. J. Am. Chem. Soc. **129:**8389–8395.
5. **Brunger, A. T.** 2007. Version 1.2 of the Crystallography and NMR system. Nat. Protoc. **2:**2728–2733.
6. **Buroni, S., G. Manina, P. Guglierame, M. R. Pasca, G. Riccardi, and E. De Rossi.** 2006. LfrR is a repressor that regulates expression of the efflux pump LfrA in *Mycobacterium smegmatis*. Antimicrob. Agents Chemother. **50:**4044–4052.
7. **Collaborative Computational Project, Number 4.** 1994. The *CCP*4 suite: programs for protein crystallography. Acta Crystallogr. D **50:**760–763.
8. **Davis, I. W., A. Leaver-Fay, V. B. Chen, J. N. Block, G. J. Kapral, X. Wang, L. W. Murray, W. B. Arendall III, J. Snoeyink, J. S. Richardson, and D. C. Richardson.** 2007. MolProbity: all-atom contacts and structure validation for proteins and nucleic acids. Nucleic Acids Res. **35:**W375–W383.
9. **DeLano, W. L.** 2002. The Pymol molecular graphics system. DeLano Scientific, Palo Alto, CA.
10. **De Rossi, E., J. A. Aínsa, and G. Riccardi.** 2006. Role of mycobacterial efflux transporters in drug resistance: an unresolved question. FEMS Microbiol. Rev. **30:**36–52.
11. **De Rossi, E., P. Arrigo, M. Bellinzoni, P. A. Silva, C. Martin, J. A. Ainsa, P. Guglierame, and G. Riccardi.** 2002. The multidrug transporters belonging to major facilitator superfamily in *Mycobacterium tuberculosis*. Mol. Med. **8:**714–724.
12. **De Silva, R. S., G. Kovacikova, W. Lin, R. K. Taylor, K. Skorupski, and F. J. Kull.** 2007. Crystal structure of the *Vibrio cholerae* quorum-sensing regulatory protein HapR. J. Bacteriol. **189:**5683–5691.
13. **Dolinsky, T. J., J. E. Nielsen, J. A. McCammon, and N. A. Baker.** 2004. PDB2PQR: an automated pipeline for the setup of Poisson-Boltzmann electrostatics calculations. Nucleic Acids Res. **32:**W665–W667.
14. **Emsley, P., and K. Cowtan.** 2004. Coot: model-building tools for molecular graphics. Acta Crystallogr. D **60:**2126–2132.
15. **Fish, D. N., and M. J. Ohlinger.** 2006. Antimicrobial resistance: factors and outcomes. Crit. Care Clin. **22:**291–311.
16. **Freire, E., A. Schön, and A. Velazquez-Campoy.** 2009. Isothermal titration calorimetry: general formalism using binding polynomials. Methods Enzymol. **455:**127–155.
17. **Günther, S., K. Rother, and C. Frömmel.** 2006. Molecular flexibility in protein-DNA interactions. BioSystems **85:**126–136.
18. **Holm, L., S. Kaariainen, P. Rosenstrom, and A. Schenkel.** 2008. Searching protein structure databases with DaliLite v. 3. Bioinformatics **24:**2780–2781.
19. **Kabsch, W.** 1988. Automatic indexing of rotation diffraction patterns. J. Appl. Crystallogr. **21:**916–924.
20. **Kalodimos, C. G., N. Biris, A. M. Bonvin, M. M. Levandoski, M. Guennuegues, R. Boelens, and R. Kaptein.** 2004. Structure and flexibility adaptation in nonspecific and specific protein-DNA complexes. Science **305:**386–389.
21. **Krissinel, E., and K. Henrick.** 2004. Secondary-structure matching (SSM), a new tool for fast protein structure alignment in three dimensions. Acta Crystallogr. D **60:**2256–2268.
22. **Li, X. Z., L. Zhang, and H. Nikaido.** 2004. Efflux pump-mediated intrinsic drug resistance in *Mycobacterium smegmatis*. Antimicrob. Agents Chemother. **48:**2415–2423.
23. **Liu, J., H. E. Takiff, and H. Nikaido.** 1996. Active efflux of fluoroquinolones in *Mycobacterium smegmatis* mediated by LfrA, a multidrug efflux pump. J. Bacteriol. **178:**3791–3795.
24. **Murshudov, G. N., A. A. Vagin, and E. J. Dodson.** 1997. Refinement of macromolecular structures by the maximum-likelihood method. Acta Crystallogr. D **53:**240–255.
25. **Niederweis, M.** 2003. Mycobacterial porins—new channel proteins in unique outer membranes. Mol. Microbiol. **49:**1167–1177.
26. **Peters, K. M., J. T. Schuman, R. A. Skurray, M. H. Brown, R. G. Brennan, and M. A. Schumacher.** 2008. QacR-cation recognition is mediated by a redundancy of residues capable of charge neutralization. Biochemistry **47:**8122–8129.
27. **Piddock, L. J.** 2006. Clinically relevant chromosomally encoded multidrug resistance efflux pumps in bacteria. Clin. Microbiol. Rev. **19:**382–402.
28. **Poole, K.** 2007. Efflux pumps as antimicrobial resistance mechanisms. Ann. Med. **39:**162–176.
29. **Ramón-García, S., C. Martín, J. A. Aínsa, and E. De Rossi.** 2006. Characterization of tetracycline resistance mediated by the efflux pump Tap from *Mycobacterium fortuitum*. J. Antimicrob. Chemother. **57:**252–259.
30. **Ramón-García, S., C. Martín, E. De Rossi, and J. A. Aínsa.** 2007. Contribution of the Rv2333c efflux pump (the Stp protein) from *Mycobacterium tuberculosis* to intrinsic antibiotic resistance in *Mycobacterium bovis* BCG. J. Antimicrob. Chemother. **59:**544–547.
31. **Ramos, J. L., M. Martinez-Bueno, A. J. Molina-Henares, W. Teran, K. Watanabe, X. D. Zhang, M. T. Gallegos, R. Brennan, and R. Tobes.** 2005. The TetR family of transcriptional repressors. Microbiol. Mol. Biol. Rev. **69:**326–356.
32. **Sander, P., E. De Rossi, B. Boddinghaus, R. Cantoni, M. Branzoni, E. C. Bottger, H. Takiff, R. Rodriquez, G. Lopez, and G. Riccardi.** 2000. Contribution of the multidrug efflux pump LfrA to innate mycobacterial drug resistance. FEMS Microbiol. Lett. **193:**19–23.
33. **Schumacher, M. A., and R. G. Brennan.** 2002. Structural mechanisms of multidrug recognition and regulation by bacterial multidrug transcription factors. Mol. Microbiol. **45:**885–893.
34. **Schumacher, M. A., M. C. Miller, and R. G. Brennan.** 2004. Structural mechanism of the simultaneous binding of two drugs to a multidrug-binding protein. EMBO J. **23:**2923–2930.
35. **Schumacher, M. A., M. C. Miller, S. Grkovic, M. H. Brown, R. A. Skurray, and R. G. Brennan.** 2002. Structural basis for cooperative DNA binding by two dimers of the multidrug-binding protein QacR. EMBO J. **21:**1210–1218.
36. **Schumacher, M. A., M. C. Miller, S. Grkovic, M. H. Brown, R. A. Skurray, and R. G. Brennan.** 2001. Structural mechanisms of QacR induction and multidrug recognition. Science **294:**2158–2163.
37. **Sheldrick, G. M.** 2008. A short history of SHELX. Acta Crystallogr. A **64:**112–122.
38. **Takiff, H. E., M. Cimino, M. C. Musso, T. Weisbrod, R. Martinez, M. B. Delgado, L. Salazar, B. R. Bloom, and W. R. Jacobs.** 1996. Efflux pump of the proton antiporter family confers low-level fluoroquinolone resistance in *Mycobacterium smegmatis*. Proc. Natl. Acad. Sci. USA **93:**362–366.
39. **Vagin, A., and A. Teplyakov.** 1997. MOLREP: an automated program for molecular replacement. J. Appl. Crystallogr. **30:**1022–1025.
40. **van den Berg, S., P. A. Löfdahl, T. Härd, and H. Berglund.** 2006. Improved solubility of TEV protease by directed evolution. J. Biotechnol. **121:**291–298.
41. **Viveiros, M., C. Leandro, and L. Amaral.** 2003. Mycobacterial efflux pumps and chemotherapeutic implications. Int. J. Antimicrob. Agents **22:**274–278.
42. **Vonrhein, C., E. Blanc, P. Roversi, and G. Bricogne.** 2007. Automated structure solution with autoSHARP. Methods Mol. Biol. **364:**215–230.